Low-threshold optical bistabilities in ultrathin nonlinear metamaterials

Shiwei Tang,[1] Baocheng Zhu,[1] Shiyi Xiao,[1] Jung-Tsung Shen,[2] and Lei Zhou[1,*]

[1]*State Key Laboratory of Surface Physics and Key Laboratory of Micro and Nano Photonic Structures (Ministry of Education), Fudan University, Shanghai 200433, China*

[2]*Department of Electrical and Systems Engineering, Washington University, St. Louis, Missouri, USA*

**Corresponding author: phzhou@fudan.edu.cn*

Received March 26, 2014; revised April 14, 2014; accepted April 16, 2014; posted April 16, 2014 (Doc. ID 209003); published May 26, 2014

Optical bistability typically occurs only when the optical thickness in the device or the input light power is unfavorably large. Here we show that, for a class of plasmonic metamaterials consisting of ultrathin holey metallic plates filled with nonlinear materials, the optical bistability can occur with an ultralow excitation power. We present a realistic design working at 0.2 THz and perform full-wave simulations to quantitatively study its optical bistability properties. An analytical model is developed to explain the inherent physics and provides a general design guideline for future development. © 2014 Optical Society of America

OCIS codes: (160.3918) Metamaterials; (190.0190) Nonlinear optics; (310.0310) Thin films; (250.5403) Plasmonics.
http://dx.doi.org/10.1364/OL.39.003212

Optical bistability is a nonlinear optical phenomenon that has potential applications in optoelectronics and logic elements such as optical switching [1], optical memories [2], optical transistors [3], optical diode [4], and optical computing [5]. Conventional optical bistability devices consist of Fabry–Perot (FP) resonators filled with nonlinear media [6–8]. To be able to sustain proper FP modes to provide the necessary feedback mechanism that amplifies the input signal, the optical thicknesses of the resonator must be at least of the order of the operating wavelength, or the input signal must be prohibitively strong [9]. Such constraints severely limit the application and the integration of optical bistable devices.

In this Letter, we show that such constrains can be relieved by combining engineered surface plasmon (SP) resonances in artificial metamaterials [10,11] with optical nonlinearity. As an illustration, we present a realistic design working at 0.2 THz, which consists of a $\lambda/25$ thick holey metallic plate with deep-subwavelength apertures filled with nonlinear medium. Finite-difference time-domain (FDTD) simulations show that optical bistability can occur in such a device with an excitation power 3500 times lower than the case of using an FP resonator of the same thickness, and the optical bistability threshold is essentially independent of the film thickness. The physics are governed by the shape resonance of the subwavelength structure, which strongly enhances the local fields inside the apertures where the nonlinear materials are embedded. We developed an analytical model that describes both the qualitative and quantitative features observed in the numerical results. Our analysis reveals the important role of plasmonic resonances in achieving such extraordinary nonlinear optical effect and provides useful design guidance for future applications.

Figure 1(a) shows a unit cell of our device, which is a 60 μm thick metallic plate (yellow region), perforated with a subwavelength aperture with a symmetrical and interconnected lateral pattern (blue region). The aperture is embedded with nonlinear material with permittivity ε_d. To illustrate the physics hereafter, we will operate the device in THz frequency domain, as the skin depth of metal is negligible, so that the metal can be considered as a perfect electric conductor. We emphasize that at frequencies wherein the loss and dispersion of metals must be taken into account, the nonlinear properties can remain qualitatively unchanged by proper optimization of the device geometry.

Figure 1(b) shows the FDTD-calculated *linear* transmission spectra of the device with varying ε_d. The incident light is polarized along the x axis (i.e., $\vec{E}\|\hat{x}$) in all

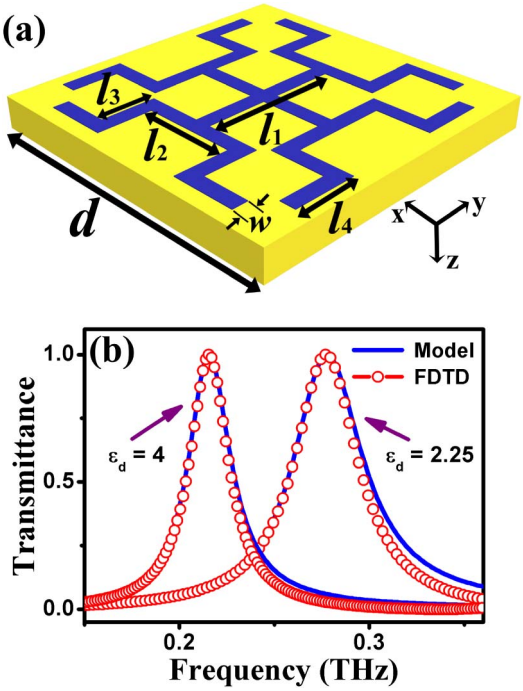

Fig. 1. (a) Schematic of the device. Shown is a unit cell with $d = 240$ μm, $l_1 = 100$ μm, $l_2 = l_3 = 40$ μm, and $l_4 = 60$ μm. The yellow (blue) region denotes the metal (nonlinear material). (b) Transmission spectra of the device with varying ε_d, calculated by FDTD simulations (circles) and the analytical model (solid lines) using Eq. (1), respectively.

calculations presented in this Letter, but we note the optical properties of the device are polarization-independent as the structure has a fourfold rotational symmetry on the xy plane. Remarkably, our numerical results indicate that the structure exhibits a perfect transmission peak at a certain frequency [12], which is redshifted when ε_d increases. Such a transparency is induced by the excitation of spoof SPs in the subwavelength-structured metallic systems [13–17]. The strong ε_d dependence of the transmission spectrum provides the capability to modulate the transmission via the input power if the embedded material is a Kerr nonlinear medium.

We exploit this feature to demonstrate the optical bistability in the device. Figure 2 plots the FDTD calculated bistable hysteresis of devices with varying thickness h and linewidth w, operating at a frequency $f = 0.2$ THz [19]. The permittivity of the Kerr medium is $\varepsilon_d = 2.25 + \chi^{(3)}|E|^2$ with $\chi^{(3)} = 1 \times 10^{-18}$ m^2/V^2, which is typical in semiconductors [20,21]. The obtained results indicate that the bistability can occur for a device that has a thickness of only 60 μm [Fig. 2(a)], which is 1/25 of the operating wavelength; also the bistability threshold field is essentially *independent* of the film thickness [Figs. 2(a) and 2(b)], but strongly depends on the linewidth w of the aperture [Figs. 2(a) and 2(c)].

To further demonstrate the ultralow threshold behavior, we employed FDTD simulations to investigate the dependence of the threshold/saturation fields on the film thickness h, for both the proposed device and a controlled case of a slab of Kerr medium of the same thickness. Since the nonlinear materials are embedded in the apertures of the metal layer, changing the metal film thickness h is equivalent to changing the nonlinear material thickness [see Fig. 1(a)]. Figure 3 clearly shows the proposed ultrathin device has a threshold that is smaller than that of an FP system by orders of magnitude. Moreover, for the proposed device, the optical bistability threshold/saturation fields exhibit qualitatively different behavior, indicating a possibly unusual governing mechanism than that in a conventional FP slab.

To gain further insight, we developed a simple analytical model to predict the optical bistable behavior of the proposed device. For the structure shown in Fig. 1(a), one can consider those subwavelength apertures (blue regions) as metallic waveguides supporting a series of eigenmodes. The wave-scattering problems related to such a structure can be rigorously solved within a general mode-expansion framework [13,22]. Under the single-mode approximation, the linear transmittance at normal incidence is given by [22,23]

$$T = \left| \frac{4Y_0 Y_{\text{hole}} e^{iq_z h}}{(Y_0 + Y_{\text{hole}})^2 - (Y_0 - Y_{\text{hole}})^2 e^{2iq_z h}} \right|^2, \quad (1)$$

where $Y_0 = k_0/\omega\mu_0$ and $Y_{\text{hole}} = q_z/S_0^2\omega\mu_0$ are the admittances of the fundamental modes in air and in the aperture waveguide, respectively; $q_z = k_0\sqrt{\varepsilon_d}\sqrt{1 - \omega_c^2/\omega^2}$, with ω_c being the cut-off frequency of the waveguide determined by the subwavelength pattern, and

$$S_0 = \frac{\int_{\text{hole}} (\vec{E}^{\text{inc}})^* \cdot (\vec{E}^{\text{wg}}) \mathrm{d}x\mathrm{d}y}{\sqrt{\int_{\text{unitcell}} |\vec{E}^{\text{inc}}|^2 \mathrm{d}x\mathrm{d}y \cdot \int_{\text{hole}} |\vec{E}^{\text{wg}}|^2 \mathrm{d}x\mathrm{d}y}} \quad (2)$$

is the overlapping integral between incident plane wave ($\vec{E}^{\text{inc}}$) and the fundamental waveguide mode ($\vec{E}^{\text{wg}}$). The parameter S_0 can be analytically solved for a simple rectangular shape and can be numerically calculated for complex aperture shapes. For our system, it is found by FDTD simulations that $S_0 = 0.22$ and $S_0 = 0.25$ for

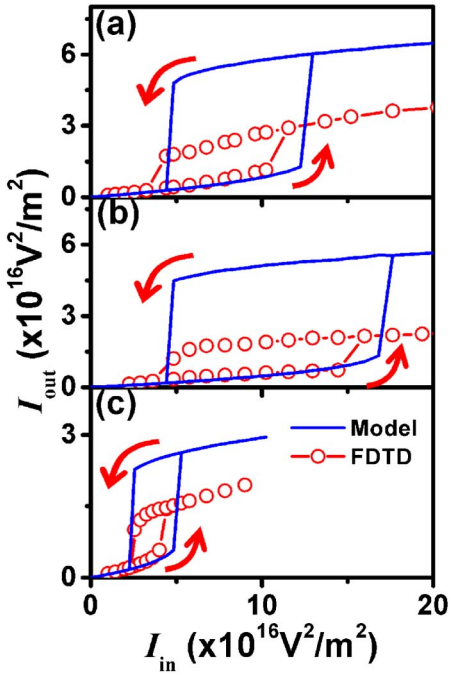

Fig. 2. Bistable hysteresis for a device with parameters (a) $w = 20$ μm, $h = 60$ μm; (b) $w = 20$ μm, $h = 80$ μm; and (c) $w = 15$ μm, $h = 60$ μm, calculated by a nonlinear FDTD scheme [18] (circles) and the analytic model calculations using Eqs. (1) and (3) (lines). Red arrows indicate the direction of the input power change.

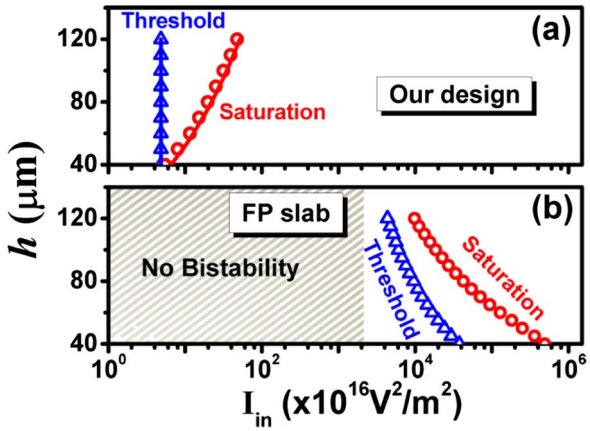

Fig. 3. Film-thickness dependences of the threshold field (blue triangles) and saturation field (red circles) for (a) our design. (b) An FP slab with the same thickness, obtained by the nonlinear FDTD calculations. Lines denote the model results calculated with Eqs. (1) and (3). The operating frequency is $f = 0.2$ THz.

the cases of $w = 15$ μm and $w = 20$ μm, respectively. Linear transmission spectra calculated using such a model are shown as solid lines in Fig. 1(b), which have excellent agreements with the FDTD results. Equation (1) shows that high transmission ($T = 1$) can be obtained when $q_z = 0$, i.e., the waveguide cut-off frequency of the aperture, which corresponds to the spoof SP resonance of the structure [23]. Since by varying ε_d the waveguide cut-off frequency ω_c is tuned, the transmission peak also shifts accordingly.

We now apply this analytical model to study the nonlinear transmissions. In nonlinear materials, ε_d can be strongly modified by the local light intensity. Different from a simple FP-slab case, here the relation between local E-field ($\vec{E}_{\rm loc}$) inside the aperture and the incident E-field ($\vec{E}_0$) is very complicated. A quantitatively accurate approximation between $\vec{E}_{\rm loc}$ and $\vec{E}_0$, however, can still be obtained by invoking the following two arguments: First, we note that $1/|S_0|^2$ essentially characterizes the Q factor of the plasmonic resonance, since S_0 represents the coupling between the plasmonic mode inside the subwavelength structure and the radiation mode in free space. Therefore, from the definition of the Q factor, the total electromagnetic (EM) energy stored inside the plasmonic cavity (e.g., the aperture) should be proportional to $|\vec{E}_0|^2 \cdot T/|S_0|^2$. Second, noticing that the EM energy is stored only inside the aperture, we can estimate the average local field as $|\vec{E}_{\rm loc}|^2 \approx A_{\rm u.c.}/A_{\rm hole} \cdot |\vec{E}_0|^2 \cdot T/|S_0|^2$ by making an area correction, where $A_{\rm u.c.}$ and $A_{\rm hole}$ represent the areas of a unit cell and an aperture, respectively. Therefore the permittivity of the Kerr medium can be written as [24]

$$\varepsilon_d = 2.25 + \chi^{(3)} \cdot \frac{A_{\rm u.c.}}{A_{\rm hole}} \cdot \frac{|\vec{E}_0|^2 \cdot T}{|S_0|^2}. \tag{3}$$

It is clear that both the Q factor of plasmonic resonance ($\sim|S_0|^{-2}$) and the aperture area correction can significantly modify the local field and thus the permittivity of the Kerr medium. In contrast, these two mechanisms do not exist in a conventional FP system so that our system exhibits distinct optical bistability behaviors. Equations (1) and (3) together form a set of coupled nonlinear equations with two unknowns (T, ε_d), which can be solved using the method developed in [7]. Precisely, by employing Eq. (1), we first computed T as functions of ε_d at the operating frequency for two different thicknesses. The results are shown as solid lines in Fig. 4. We note that high transmission ($T \sim 1$) only occurs at a particular ε_d value for which case the waveguide cut-off frequency is equal to the operating one. We then used Eq. (3) to obtain $T(\varepsilon_d)$ (which is a straight line as this is a linear relation) for varying input power. The results are shown by the dashed lines in Fig. 4. According to Eq. (3), the slopes of $T(\varepsilon_d)$ are proportional to the inverse of the input power (i.e., $|\vec{E}_0|^{-2}$). Therefore the crossing points of these two curves are the graphical representations of the solutions of Eqs. (1) and (3).

Such a graphical method proves to be helpful in understanding the properties of the device in a simple and direct manner [Fig. (4)]. For example, the threshold

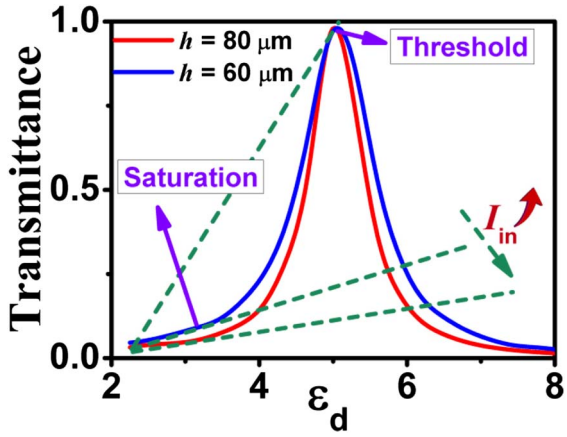

Fig. 4. Graphical representation and determination of the optical bistability threshold and saturation fields for different thicknesses. Solid and dashed lines are calculated by Eqs. (1) and (3), respectively.

of the input power is wherein the straight line begins to contact the transmission spectrum from above (so that the solutions start to be in existence); the saturation field corresponds to the input power for which the straight line ceases to have two intersections with the transmission curve, yielding only one crossing point. We note that from Eq. (1), the spectral positions of the transmission peaks are not sensitive to the film thickness h, as the high transmission is mainly induced by the waveguided mode at cutoff in the apertures; the nature of this mode is a lateral resonance on the xy plane. As a result, the optical bistability threshold is also nearly independent on h as long as the lateral structure (the aperture) is unchanged. On the other hand, the saturation field has a stronger dependence on h, since the transmission peak is narrowed when h is increased (Fig. 4).

Alternatively, if the aperture linewidth w is decreased while all other structural parameters are unchanged, the overlapping integral S_0 will be reduced, leading to an enhanced plasmonic Q factor; thus the required input field should also be decreased so that the straight line according to Eq. (3) can keep the same slope. This explains why the threshold and saturation fields are reduced for a device with a smaller w [see Fig. 2(c)], since the local field inside the aperture is significantly enhanced by such lateral field squeezing mechanism [see Eq. (3)]. In contrast, the resonance peak in an FP slab strongly depends on the slab thickness h, and there is no such mechanism to significantly enhance the local field in the transverse direction inside a FP slab. Therefore an FP slab yields qualitatively different optical bistability behaviors. In Figs. (1)–(3), we also plot the results according to the analytic model, compared with the rigorous FDTD ones. The agreements in Figs. (1)–(3) are in general acceptable.

We note from Fig. 2 that the analytic model overestimates the transmitted signals as compared with the FDTD results, although it can well reproduce the threshold/saturation fields. It is because that the incident E field oscillates in time so that ε_d is also a fast oscillating

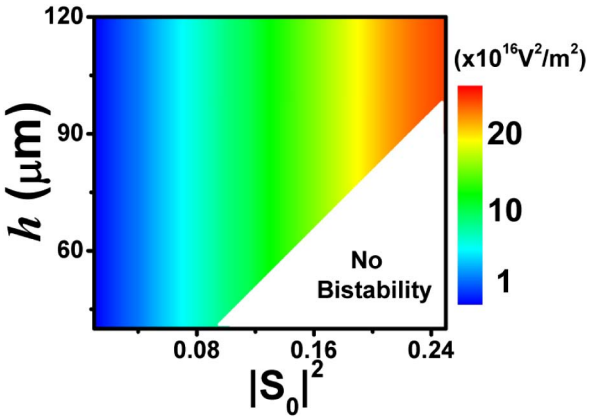

Fig. 5. Optical bistability threshold as a function of S_0 and h.

function of time. Such an oscillation gives rise to the so-called self-phase modulation [25] in a Kerr medium, which is known to broaden the transmission/reflection spectral even when the incident light is strictly monochromatic. Therefore the transmittance at the carrier frequency should be correctively reduced to account for the portion of the light energy that has been transferred to other frequency components.

As the analytic model only involves two parameters (S_0 and h), we can optimize the geometry of the device in the parameter space of S_0 and h to minimize the optical bistability threshold. Figure 5 shows the optical bistability threshold as a function of S_0 and h. The result indicates that the threshold decreases when S_0 becomes smaller but is essentially independent of h. Therefore a strategy to decrease the optical bistability threshold is to decrease S_0 yet keeping the resonance frequency unchanged; this is because the Q factor of the plasmonic resonance is enhanced as S_0 decreases.

This analysis provides guidance to design the appropriate aperture shape. For example, it can be shown that a square-shaped aperture would not work. For a square shape, analytical calculation shows that $S_0 = 2\sqrt{2}a/\pi d$ and $\omega_c = c\pi/(a\sqrt{\varepsilon_d})$, with a being the side length of the square hole and d the period [23]. While we can make S_0 small by decreasing a, the resonance frequency ω_c, however, increases at the same time; to keep ω_c unchanged, the linear part of ε_d has to increase significantly, which is not easy to realize in practice. In contrast, more complicated shapes such as a fractal in Fig. 1 provides an additional freedom, i.e., the linewidth w, to allow the decreasing S_0 without affecting ω_c.

In summary, by combining the engineered SP resonance with nonlinearity, a new mechanism emerges that allows achieving optical bistability at an ultralow threshold in an ultrathin device at deep subwavelength scales. Such an approach could be promising for the design and the realization of highly superior and ultracompact optical bistable devices.

This work was supported by the NSFC (no. 11174055), Program of Shanghai Subject Chief Scientist (12XD1400700) and MOE of China (no. B06011).

References and Notes

1. D. A. Mazurenko, R. Kerst, and J. I. Dijkhuis, Phys. Rev. Lett. **91**, 213903 (2003).
2. H. Nihei and A. Okamoto, Jpn. J. Appl. Phys. **40**, 6835 (2001).
3. G. Assanto, Z. Wang, D. J. Hagan, and E. W. Van Stryland, Appl. Phys. Lett. **67**, 2120 (1995).
4. M. D. Tocci, M. J. Bloemer, M. Scalora, J. P. Dowling, and C. M. Bowden, Appl. Phys. Lett. **66**, 2324 (1995).
5. I. S. Nefedov, V. N. Gusyatnikov, and P. K. Kashkarov, Laser Phys. **10**, 640 (2000).
6. M. Born and E. Wolf, *Principles of Optics*, 4th ed. (Pergamon, 1970).
7. F. S. Felber and J. H. Marburger, Appl. Phys. Lett. **28**, 731 (1976).
8. J. H. Marburger and F. S. Felber, Phys. Rev. A **17**, 335 (1978).
9. W. Chen and D. L. Mills, Phys. Rev. B **35**, 524 (1987).
10. T. W. Ebbesen, H. J. Lezec, H. F. Ghaemi, T. Thio, and P. A. Wolff, Nature **391**, 667 (1998).
11. W. L. Barnes, A. Dereux, and T. W. Ebbesen, Nature **424**, 824 (2003).
12. The transmittance is less than 100% when metallic losses are taken into account.
13. F. J. Garcia-Vidal, L. Martín-Moreno, and J. B. Pendry, J. Opt. A Pure Appl. Opt. **7**, S97 (2005).
14. A. B. Khanikaev, S. H. Mousavi, G. Shvets, and Y. S. Kivshar, Phys. Rev. Lett. **105**, 1 (2010).
15. N. F. Yu, Q. J. Wang, M. A. Kats, J. A. Fan, S. P. Khanna, L. Li, A. G. Davies, E. H. Linfield, and F. Capasso, Nat. Mater. **9**, 730 (2010).
16. Y. Ueba, J. Takahara, and T. Nagatsuma, Opt. Lett. **36**, 909 (2011).
17. D. Martin-Cano, O. Quevedo-Teruel, E. Moreno, L. Martin-Moreno, and F. J. Garcia-Vidal, Opt. Lett. **36**, 4635 (2011).
18. EastFDTD V4.0, DONGJUN Science and Technology Co., China.
19. Calculations show that the working bandwidth of the device is about 19 GHz.
20. A. Mayer and F. Keilmann, Phys. Rev. B **33**, 6962 (1986).
21. R. Brazis, R. Raguotis, and M. R. Siegrist, J. Appl. Phys. **84**, 3474 (1998).
22. S. Y. Xiao, Q. He, X. Q. Huang, and L. Zhou, Metamaterials **5**, 112 (2011).
23. J. Jung, F. J. Garcia-Vidal, L. Martin-Moreno, and J. B. Pendry, Phys. Rev. B **79**, 153407 (2009).
24. Such a relation can also be rigorously derived from the mode-expansion theory under the single-mode approximation.
25. G. P. Agrawal and N. A. Olsson, IEEE JQE **25**, 2297 (1989).